

The Dynamics of Noble Metal Atom Penetration through Methoxy-Terminated Alkanethiolate Monolayers

Amy V. Walker,^{*,†} Timothy B. Tighe, Orlando M. Cabarcos, Michael D. Reinard, Brendan C. Haynie, Sundararajan Uppili, Nicholas Winograd,^{*} and David L. Allara^{*}

Contribution from the Department of Chemistry, Pennsylvania State University, 184 Materials Research Institute, University Park, Pennsylvania 16802

Received November 13, 2003; E-mail: nxw@psu.edu; dla3@psu.edu; walker@wustl.edu

Abstract: We have studied the interaction of vapor-deposited Al, Cu, Ag, and Au atoms on a methoxy-terminated self-assembled monolayer (SAM) of HS(CH₂)₁₆OCH₃ on polycrystalline Au{111}. Time-of-flight secondary ion mass spectrometry, infrared reflection spectroscopy, and X-ray photoelectron spectroscopy measurements at increasing coverages of metal show that for Cu and Ag deposition at all coverages the metal atoms continuously partition into competitive pathways: penetration through the SAM to the S/substrate interface and solvation-like interaction with the -OCH₃ terminal groups. Deposited Au atoms, however, undergo only continuous penetration, even at high coverages, leaving the SAM "floating" on the Au surface. These results contrast with earlier investigations of Al deposition on a methyl-terminated SAM where metal atom penetration to the Au/S interface ceases abruptly after a ~1:1 Al/Au layer has been attained. These observations are interpreted in terms of a thermally activated penetration mechanism involving dynamic formation of diffusion channels in the SAM via hopping of alkanethiolate-metal (RSM-) moieties across the surface. Using supporting quantum chemical calculations, we rationalized the results in terms of the relative heights of the hopping barriers, RSAI > RSAg, RSCu > RSAu, and the magnitudes of the metal-OCH₃ solvation energies.

1. Introduction

Understanding the atomic and molecular level interaction of metal atoms with organic surfaces is becoming increasingly important as the number of applications involving metal-organic interfaces grows. In addition to the longstanding general interest in metallization of polymers,¹⁻³ of particular interest recently has been the emergence of the fields of polymer and molecular electronic devices⁴⁻¹⁶ in which the issue of optimizing

top metal contacts is of critical importance.¹⁷ Given the complexity of these structures in terms of chemical interactions and metal film morphology and given the wide range of choices in metals, organic materials, and deposition conditions, the rational design of metal-organic structures requires a broad, fundamental understanding of the mechanistic and thermodynamic aspects of metal atom-molecule interactions. The spectrum of interactions can be quite varied, ranging from weak adsorption, which could lead to clustering with poor adhesion and/or electrical contact, and diffusion into the bulk, to strong chemical reaction with severe destruction of chemical integrity.

Recent efforts to explore fundamental interactions have focused on the use of self-assembled monolayers (SAMs) because of their highly organized surface structures with uniform density of organic groups that allow quantitative characterization of the metal-molecule interactions.¹⁸⁻²⁸ This approach is directly relevant to molecular electronic devices whose core

[†] Present address: Department of Chemistry, Washington University in St. Louis, Campus Box 1134, St. Louis, MO 63130.

- (1) Pireaux, J. J. *Synth. Met.* **1994**, *67*, 39-46.
- (2) Strunksus, T.; Grunze, M.; Kochendoerfer, G.; Wöll, Ch. *Langmuir* **1996**, *12*, 2712-2725.
- (3) Faupel, F.; Willecke, R.; Thran, A. *Mater. Sci. Eng.* **1998**, *R22*, 1-55.
- (4) Service, R. F. *Science* **1996**, *273*, 878-880.
- (5) Zhou, C.; Deshpande, M. R.; Reed, M. A.; Jones, L., II; Tour, J. M. *Appl. Phys. Lett.* **1997**, *71*, 611-613.
- (6) Reed, M. A. *Proc. IEEE* **1999**, *87*, 652-658.
- (7) Chen, J.; Reed, M. A.; Rawlett, A. M.; Tour, J. M. *Science*, **1999**, *286*, 1550-1552.
- (8) Friend, R.; Burroughes, J.; Shimoda, T. *Physics World*, June 1999, pp 35-40.
- (9) Friend, R. H.; Gymer, G. W.; Holmes, A. B.; Burroughes, J. H.; Marks, R. N.; Taliani, C.; Bradley, D. D. C.; Dos Santos, D. A.; Brédas, J. L.; Lögdlund, M.; Salaneck, W. R. *Nature* **1999**, *397*, 121-128.
- (10) Bumm, L. A.; Arnold, J. J.; Dunbar, T. D.; Allara, D. L.; Weiss, P. S. J. *Phys. Chem. B* **1999**, *103*, 8122-8127.
- (11) Tour, J. M. *Acc. Chem. Res.* **2000**, *33*, 791-804.
- (12) Reed, M. A.; Chen, J.; Rawlett, A. M.; Price, D. W.; Tour, J. M.; *Appl. Phys. Lett.* **2001**, *78*, 3735-3637.
- (13) Xu, T.; Peyerson, I. R.; Lakshikantham, M. V.; Metzger, R. M. *Angew. Chem., Int. Ed.* **2001**, *40*, 1749-1752.
- (14) Metzger, R. M.; Xu, T.; Peterson, I. R. *J. Phys. Chem. B* **2001**, *105*, 7280-7290.
- (15) Liang, W.; Shores, M. P.; Bockrath, M.; Long, J. R.; Park, H. *Nature* **2002**, *417*, 725-729.
- (16) Babel, A.; Jenekhe, S. A. *J. Phys. Chem. B* **2002**, *106*, 6129-6132.

- (17) Allara, D. L.; Dunbar, T. D.; Weiss, P. S.; Bumm, L. A.; Cygan, M. T.; Tour, J. M.; Reinert, W. A.; Yao, Y.; Kozaki, M.; Jones, L., II. *Ann. N.Y. Acad. Sci.* **1998**, *852*, 349-370.
- (18) Tarlov, M. J. *Langmuir* **1992**, *8*, 80-89.
- (19) Jung, D. R.; Czanderna, A. W. *Crit. Rev. Solid State Sci.* **1994**, *19*, 1-54.
- (20) Konstadinis, K.; Zhang, P.; Opila, R. L.; Allara, D. L. *Surf. Sci.* **1995**, *338*, 300-312.
- (21) Jung, D. R.; Czanderna, A. W. *Z. Phys. Chem.* **1997**, *20*, 163-196.
- (22) Jung, D. R.; Czanderna, A. W.; Herdt, G. C. *J. Vac. Sci. Technol., A* **1996**, *14*, 1779-1787.
- (23) Herdt, G. C.; Czanderna, A. W. *J. Vac. Sci. Technol., A* **1997**, *15*, 513-519.
- (24) Herdt, G. C.; Czanderna, A. W. *J. Vac. Sci. Technol., A* **1999**, *17*, 3415-3418.
- (25) Dake, L. S.; King, D. E.; Czanderna, A. W. *Solid State Sci.* **2000**, *2*, 781-789.

structures depend on SAMs, typically with vacuum-deposited metal contacts.^{7,14} On a more fundamental level, these types of experiments add a new strategy to the study of organometallic chemistry by providing quantitative probes of nascent metal atom interactions with organic functional groups in well-defined geometries under highly controlled conditions. In particular, this strategy complements current studies of solvation and electron-transfer reactions of metal atoms with gas-phase molecules and clusters.^{29–31} Of special significance in the metal-SAM experiments is the ability to control the orientations and spacing of the organic groups presented to the metal atoms, as opposed to the unconstrained geometries in the 3-D gas-phase experiments.

Recently we have reported on the interaction of vapor-deposited Al atoms with a selected range of common O-containing groups, including $-\text{CO}_2\text{CH}_3$,²⁶ $-\text{COOH}$,²⁷ $-\text{OH}$,²⁸ and $-\text{OCH}_3$ ²⁸ along with control experiments on $-\text{CH}_3$.²⁸ Aluminum was chosen as a metal because of its common use in microelectronics applications, its well-known organometallic chemistry with O-containing molecules,³² and our discovery that over the range of functional groups surveyed Al displays a wide range of chemical and physical interactions. The latter point is illustrated by the observations that vapor-deposited Al can react to form organoaluminum complexes ($-\text{CO}_2\text{CH}_3$, $-\text{COOH}$, and $-\text{OH}$), penetrate to the Au/S interface ($-\text{CH}_3$), or both penetrate to the Au/S interface and be weakly stabilized by the terminal group at the SAM/vacuum interface ($-\text{OCH}_3$).²⁸ The Al metal atom penetration into the $-\text{CH}_3$ ²⁶ and $-\text{OCH}_3$ ²⁸ terminated SAMs was proposed to occur via thermally activated lateral hopping of the S atom of the alkanethiolate from favorable Au adsorption sites, which leads to the creation of transient holes allowing transport of nearby Al atoms directly to the S/Au interface.^{26,28}

The case of the $-\text{OCH}_3$ terminated SAM²⁸ is of particular value since this group displays an intermediate reactivity between the limiting cases of $-\text{CH}_3$, where Al penetrates to the Au/S interface, and $-\text{COOH}$, $-\text{CO}_2\text{CH}_3$, and $-\text{OH}$ cases, where Al interacts solely with the terminus. Thus, an $-\text{OCH}_3$ terminated SAM should be an ideal case for a study of the relationship between the detailed metal–molecule interactions at the vacuum interface and variations in the metal atoms deposited. Since the noble metals are of great interest in electronics applications due to their electrical conductivity and general inertness, they are of prime interest for such a study to complement Al, which is widely used in microelectronics. Gold is primarily employed for ohmic contacts,³³ while copper and silver are widely used for wiring.³⁴ Since the mid-1990s, copper has also been employed to interconnect layers in microchips. This technology has started to supplant traditional aluminum metallization.³⁵

In this paper, we investigate the interaction of vapor-deposited Ag, Cu, and Au with a methoxy-terminated SAM and determine the mechanism of metal atom penetration through the SAM. Infrared reflection spectroscopy (IRS) and time-of-flight secondary-ion-mass-spectrometry (TOF SIMS) are used as primary in situ tools, along with X-ray photoelectron spectroscopy (XPS) to characterize the chemical and physical interactions of the metal atoms with the SAM as a function of varying metal atom coverage. The results show that under our experimental conditions deposited Cu and Ag atoms, independent of coverage, partition between solvation types of interactions with the $-\text{OCH}_3$ terminal groups³⁶ and penetration to the Au/S interface. In the case of Au deposition, however, no selective interaction with the terminal group is observed, and the deposited metal atoms penetrate to the Au/S interface, independent of coverage. These results are compared with those obtained previously for Al interacting with the $-\text{OCH}_3$ terminated SAM in which the partitioning between stabilization at the $-\text{OCH}_3$ surface and penetration into the SAM ceases abruptly at ~ 1 Al deposited per Au surface atom.²⁸ Aided by quantum chemical calculations, an interpretation of these results is made on the basis of a general mechanism involving dynamic competitions between metal–molecule interactions and the rates of fluctuations of chain hopping controlled by the barrier heights for diffusion of metal–thiolate complexes on the gold substrate.

2. Experimental Section

2.1. Materials and General Procedures. The preparation and characterization of SAMs used in this study has been described in detail previously.^{28,37–45} The metals for all depositions were obtained from different sources (Goodfellow, R. D. Mathis, Alfa Aesar, Sigma Aldrich) but were of greater than 99.99% purity in all cases.

2.2. SAM Preparation. Films of Cr (~ 5 nm) and Au (~ 200 nm) were thermally deposited sequentially onto clean Si(001) native oxide covered wafers. Self-assembly of well-organized monolayers was achieved by immersing the Au substrates into millimolar solutions of the relevant hexadecanethiol molecules in absolute ethanol for ~ 2 days at ambient temperature. The monolayer films were characterized with single wavelength ellipsometry, infrared spectroscopy, and contact angle measurements to ensure that they were densely packed, clean surfaces. In addition, all SAMs were characterized by TOF SIMS, XPS, and IRS measurements prior to metal deposition.

2.3. Time-of-Flight Secondary Ion Mass Spectrometry. The TOF SIMS analyses were performed on a custom designed instrument as described previously.⁴⁶ Briefly, the instrument consisted of a loadlock, a preparation chamber, a metal deposition chamber, and the primary

- (26) Hooper, A.; Fisher, G. L.; Konstantinidia, K.; Jung, D.; Nguyen, H.; Opila, R.; Collins, R. W.; Winograd, N.; Allara, D. L. *J. Am. Chem. Soc.* **1999**, *121*, 8052–8064.
 (27) Fisher, G. L.; Hooper, A. E.; Opila, R. L.; Allara, D. L.; Winograd, N. *J. Phys. Chem. B* **2000**, *104*, 3267–3273.
 (28) Fisher, G. L.; Walker, A. V.; Hooper, A. E.; Tighe, T. B.; Bahnck, K. B.; Skriba, H. T.; Reinard, M. D.; Haynie, B. C.; Opila, R. L.; Winograd, N.; Allara, D. L. *J. Am. Chem. Soc.* **2002**, *124*, 5528–5541.
 (29) Lisy, J. M. *Int. Rev. Phys. Chem.* **1997**, *16*, 267–289.
 (30) Niedner-Schatteburg, G.; Bondybey, V. E. *Chem. Rev.* **2000**, *100*, 4059–4086.
 (31) Duncan, M. A. *Int. J. Mass Spectrom.* **2000**, *200*, 545–569.
 (32) Cotton, F. A.; Wilkinson, G.; Murillo, C. A.; Bochmann, M.; *Advanced Inorganic Chemistry*, 6th ed.; John Wiley & Sons: New York, 1999.
 (33) Tachibana, T.; Williams, B. E.; Glass, J. T. *Phys. Rev. B* **1992**, *45*, 11968–11974.
 (34) Angelopoulos, M. *IBM J. Res. Dev.* **2001**, *45*, 57–75.

- (35) Monteiro, O. R. *J. Vac. Sci. Technol., B* **1999**, *17*, 1094–1097.
 (36) Walker, A. V.; Tighe, T. B.; Reinard, M. D.; Haynie, B. C.; Allara, D. L.; Winograd, N. *Chem. Phys. Lett.* **2003**, *369*, 615–620.
 (37) Nuzzo, R. G.; Allara, D. L. *J. Am. Chem. Soc.* **1983**, *105*, 4481–4483.
 (38) Bain, C. D. Self-Assembled Monolayer Films of Thiols on Gold, Ph.D. Thesis, Harvard University, Cambridge, MA, 1989.
 (39) Nuzzo, R. G.; Dubois, L. H.; Allara, D. L. *J. Am. Chem. Soc.* **1990**, *112*, 558–569.
 (40) Laibinis, P. E.; Whitesides, G. M.; Allara, D. L.; Tao, Y. T.; Parikh, A. N.; Nuzzo, R. G. *J. Am. Chem. Soc.* **1991**, *113*, 7152–7167.
 (41) Xu, C. J.; Sun, L.; Kepley, L. J.; Crooks, R. M.; Ricco, A. J. *Anal. Chem.* **1993**, *65*, 2102–2107.
 (42) Laibinis, P. E.; Bain, C. D.; Nuzzo, R. G.; Whitesides, G. M. *J. Phys. Chem.* **1995**, *99*, 7663–7676.
 (43) Tour, J. M.; Jones, L. II; Pearson, D. L.; Lamba, J. J. S.; Burgin, T. P.; Whitesides, G. M.; Allara, D. L.; Parikh, A. N.; Atre, S. V. *J. Am. Chem. Soc.* **1995**, *117*, 9529–9534.
 (44) Fryxell, G. E.; Rieke, P. C.; Halverson, A. *Langmuir* **1996**, *12*, 5064–5075.
 (45) Leff, D. V.; Brandt, L.; Heath, J. R. *Langmuir* **1996**, *12*, 4723–4730.
 (46) Braun, R. M.; Blenkinsopp, P.; Mullock, S. J.; Corlett, C.; Willey, K. F.; Vickerman, J. C.; Winograd, N. *Rapid Commun. Mass. Spectrom.* **1998**, *12*, 1246–1252.

analysis chamber, each separated by a gate valve. The primary Ga^+ ions were accelerated to 15 keV and contained in a 100-nm diameter probe beam, which was rastered over a $(106 \times 106) \mu\text{m}^2$ area during data acquisition. All spectra were acquired using a total ion dose of less than 10^{11} ions cm^{-2} . Relative peak intensities were reproducible to within $\pm 8\%$ from sample to sample and $\pm 8\%$ from scan to scan.

The metals were deposited onto the sample at room temperature from a W-wire basket source at a rate of ~ 0.15 atoms $\text{nm}^{-2} \text{s}^{-1}$ with the pressure below 5×10^{-8} Torr. After deposition, the preparation chamber pressure was allowed to recover to the base value of 1.5×10^{-9} Torr before sample transfer to the analysis chamber. The deposited mass/area was monitored using a Maxtek, Inc. TM-400 quartz crystal microbalance (QCM) controller with a maximum error within $\pm 8\%$.

2.4. Infrared Spectroscopy. Analyses were performed on a Fourier transform instrument (Mattson Research Series 1000) fitted with custom in-house optics configured external to the instrument and designed for grazing incidence reflection of samples under vacuum.^{26–28} A liquid nitrogen-cooled MCT detector was used with an effective low-frequency cutoff of $\sim 750 \text{ cm}^{-1}$. The infrared beam was allowed to access the vacuum system and reflect from the sample through a pair of differentially pumped KBr windows. After analysis of the bare monolayer, a shield was moved to unblock the path between the sample and the metal source. The metals were evaporated from a W-wire basket at a rate of ~ 0.15 atoms $\text{nm}^{-2} \text{s}^{-1}$ as measured by a QCM. The pressure remained below 1×10^{-7} Torr during the deposition.

2.5. X-ray Photoelectron Spectroscopy. The XPS analyses were performed on a spectrometer (Scienta ESCA 300) equipped with a monochromatic Al $K\alpha$ source, as described in detail elsewhere.^{47,48} Data were taken at a photoelectron takeoff angle of 15° from the sample surface with a pass energy of 75 eV and an energy step of 0.05 eV. The resulting full width at half-maximum (fwhm) for Au $4f_{7/2}$ is 0.52 eV. A binding energy of 84.00 eV for Au $4f_{7/2}$ was used as a reference for all spectra.

Following analysis of the bare monolayer, the sample was transferred under vacuum to the deposition chamber, which was isolated from the analysis chamber by a gate valve. The pressure in the preparation chamber remained below 5×10^{-8} Torr during the deposition. Incremental amounts of aluminum and silver were deposited at a highly controlled, constant rate, typically ~ 0.15 atoms $\text{nm}^{-2} \text{s}^{-1}$ as monitored by a QCM, by evaporation from a graphite crucible heated to 1248 and 1198 K, respectively. After deposition, the metal–SAM specimen was transferred directly under vacuum to the analysis chamber where the pressure was maintained below 1×10^{-8} Torr.

2.6. Quantum Chemistry Calculations. Density functional theory (DFT) calculations were performed to provide estimates of the interactions of Al, Cu, Ag, and Au atoms with the $-\text{OCH}_3$ and $-\text{S}$ moieties of the molecules. All calculations were carried out using the Gaussian 98 program package.⁴⁹

In the case of the metal–S interactions, the SAM molecule was truncated by 11 methylene units and modeled as $\text{CH}_3\text{O}-(\text{CH}_2)_5-\text{SH}$ to reduce the computational cost. This simplification is not expected

to significantly affect the calculated bond energies since intramolecular induction effects typically range over 2–3 bonds. Geometry optimizations and frequency calculations were performed at the B3PW91/LANL2DZ level of theory. The LANL2DZ basis sets, which use an effective core potential (ECP), were used to reduce explicit consideration of the large number of electrons in the metal atoms. It has been demonstrated that calculations using ECPs compare well with full electron calculations in the case of several small Au-, Ag-, and Cu-containing molecules⁵⁰ as well as in several S–Au species.⁵¹ All energies are reported as enthalpies of the final structures relative to the isolated reactants and contain zero-point energy corrections and thermal energy corrections for standard temperature and pressure.

For computational efficiency in achieving accurate interaction energies between the metal atoms and the $-\text{OCH}_3$ group, small model systems of $\text{M} + \text{CH}_3\text{OCH}_3$ and $\text{CH}_3\text{CH}_2\text{CH}_3$ were used, where $\text{M} = \text{Al}, \text{Cu}, \text{Ag},$ and Au . The most accurate results were obtained for Al atom complexes since the smaller number of electrons in comparison to Cu, Ag, and Au allowed the use of larger basis sets. Geometry optimizations for these Al model systems were performed using the B3PW91 functional with the 6-311+G(2df,p) and the LANL2DZ basis sets. Aluminum interaction energies using the B3PW91/6-311+G(2df,p) level of theory compare well to those calculated for Al with water^{52,53} and dimethyl ether⁵⁴ using MP, quadratic configuration interaction (QCI) and coupled cluster (CC) methodologies,^{52–54} and experimentally derived values.⁵⁵ The Au, Ag, and Cu complexes were run solely at the B3PW91/LANL2DZ level. The interaction energy of the model system with Al, Cu, Ag, and Au were determined as the relative energy of the geometry-optimized complex with respect to the energies of the optimized components. Additionally, thermal and zero-point energy corrections were obtained from frequency calculations.

2.7. Definition of Deposited Metal Coverage. The metal deposition onto the samples was monitored directly as the mass per unit area by a QCM. For ease in data analysis and interpretation, the deposited amounts were converted to coverage of metal atoms per SAM molecule, designated θ_{M} ($\text{M} = \text{Al}, \text{Cu}, \text{Ag}, \text{Au}$). The SAM molecular density is 4.6 molecules nm^{-2} in a well-formed alkanethiolate on Au{111}.⁵⁶ Thus, for $\theta_{\text{M}} = 1.0$ there would be one metal atom deposited on average per SAM molecule.

3. Results

Results for the deposition of Al on $-\text{OCH}_3$ terminated SAMS have been reported in detail previously²⁸ and are included here for comparison purposes.

3.1. TOF SIMS. A detailed discussion of the positive and negative ion mass spectra of the bare $-\text{OCH}_3$ monolayer has been presented previously.²⁸ In agreement with this earlier work,^{26–28,57–60} we find that the relative intensities of Au_x^- , Au_xS_y^- , and SO_z^- (where $Z = 1–4$) provide a useful indication that the SAM was prepared without substantial incorporation of impurities or oxidative products.

- (47) Beamson, G.; Briggs, D.; Davies, S. F.; Fletcher, I. W.; Cark, D. T.; Howard, J.; Gelius, U.; Wannberg, B.; Balzer, P. *Surf. Interface Anal.* **1990**, *15*, 541–549.
- (48) Gelius, U.; Wannberg, B.; Baltzer, P.; Fellnerfeldegg, H.; Carlsson, G.; Johansson, C. G.; Larsson, J.; Munger, P.; Vegerfors, G. *J. Electron Spectrosc. Relat. Phenom.* **1990**, *52*, 747–785.
- (49) Frisch, M. J.; Trucks, G. W.; Schlegel, H. B.; Scuseria, G. E.; Robb, M. A.; Cheeseman, J. R.; Zakrzewski, V. G.; Montgomery, J. A., Jr.; Stratmann, R. E.; Burant, J. C.; Dapprich, S.; Millam, J. M.; Daniels, A. D.; Kudin, K. N.; Strain, M. C.; Farkas, O.; Tomasi, J.; Barone, V.; Cossi, M.; Cammi, R.; Mennucci, B.; Pomelli, C.; Adamo, C.; Clifford, S.; Ochterski, J.; Petersson, G. A.; Ayala, P. Y.; Cui, Q.; Morokuma, K.; Malick, D. K.; Rabuck, A. D.; Raghavachari, K.; Foresman, J. B.; Cioslowski, J.; Ortiz, J. V.; Stefanov, B. B.; Liu, G.; Liashenko, A.; Piskorz, P.; Komaromi, I.; Gomperts, R.; Martin, R. L.; Fox, D. J.; Keith, T.; Al-Laham, M. A.; Peng, C. Y.; Nanayakkara, A.; Gonzalez, C.; Challacombe, M.; Gill, P. M. W.; Johnson, B. G.; Chen, W.; Wong, M. W.; Andres, J. L.; Head-Gordon, M.; Replogle, E. S.; Pople, J. A. *Gaussian 98*, revision A.9; Gaussian, Inc.: Pittsburgh, PA, 1998.

- (50) Legge, F. S.; Nyberg, G. L.; Peel, J. B. *J. Phys. Chem. A* **2001**, *105*, 7905–7916.
- (51) (a) Seminario, J. M.; Zacarias, A. G.; Tour, J. M. *J. Phys. Chem. A* **1999**, *103*, 7883–7887. (b) Seminario, J. M.; Zacarias, A. G.; Tour, J. M. *J. Am. Chem. Soc.* **1999**, *121*, 411–416.
- (52) Fängström, T.; Lunell, S.; Kasai, P. H.; Eriksson, L. A. *J. Phys. Chem. A* **1998**, *102*, 1005–1007.
- (53) Sakai, S. *J. Phys. Chem.* **1992**, *96*, 8369–8373.
- (54) Sakai, S. *J. Phys. Chem.* **1993**, *97*, 8917–8921.
- (55) Parnis, J. M.; Mitchell, S. A.; Rayner, D. M.; Hackett, P. A. *J. Phys. Chem.* **1988**, *92*, 3869–3874.
- (56) Dubois, L. H.; Nuzzo, R. G. *Annu. Rev. Phys. Chem.* **1992**, *43*, 437–463.
- (57) Tarlov, M. J.; Neuman, J. G. *Langmuir* **1992**, *8*, 1398–1405.
- (58) Hagenhoff, B.; Benninghoven, A.; Spinke, J.; Liley, M.; Knoll, W. *Langmuir* **1993**, *9*, 1622–1624.
- (59) Wood, M. C. Surface Characterization and Imaging with Ion-Induced Desorption and Multiphoton Resonance Ionization. Ph.D. Thesis, The Pennsylvania State University, University Park, PA, 1995.
- (60) Hooper, D. A.; Cooper, E.; Leggett, G. J. *J. Phys. Chem. B* **1998**, *102*, 174–184.

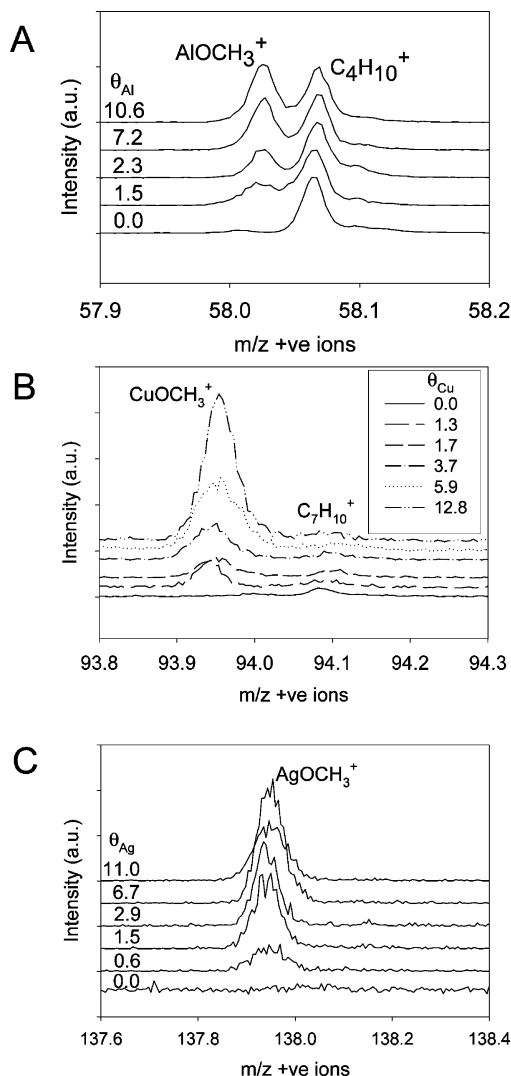


Figure 1. High-resolution SIMS spectral overlays of MOCH_3^+ fragments. A, B, and C represent positive ions of nominal mass 58, 94, and 138 amu. The intensities in plots A and B are normalized to the initial peak intensity of $\text{C}_4\text{H}_{10}^+$ and $\text{C}_7\text{H}_{10}^+$, respectively.

3.1.1. Deposition of Al, Cu, and Ag. The positive ion mass spectra show evidence that the metal atoms interact with the terminal $-\text{OCH}_3$ group. Specifically, in Figure 1, the intensity of the MOCH_3^+ ($m/z = 58, 94, 138$, respectively) peaks, indicative of metal $-\text{OCH}_3$, increase with increasing values of θ_M , where $M = \text{Al, Cu, Ag}$. The AlOCH_3^+ and CuOCH_3^+ spectra are normalized to the initial peak intensities of $\text{C}_4\text{H}_{10}^+$ and $\text{C}_7\text{H}_{10}^+$, respectively, to make obvious the changing intensities of the peaks with respect to the hydrocarbon fragments as the deposition progresses. No $\text{M}_x\text{O}_y^{\pm}$ ions were observed (data not shown). On the basis of our previous work with $-\text{CO}_2\text{H}$,²⁷ $-\text{OCH}_3$,²⁸ and $-\text{CO}_2\text{CH}_3$,²⁶ the appearance of MOCH_3^+ ions but not $\text{M}_x\text{O}_y^{\pm}$ ions indicates that the deposited metal has not undergone a redox interaction with the methoxy functionality to form $\text{M}-\text{O}$ bonds, but signifies that the deposited metal atoms have only weakly interacted with the terminal group and are stabilized at the SAM interface.

The metal atoms cannot exclusively be stabilized at the SAM surface since the data also show evidence for the penetration of the Al, Cu, or Ag atoms to the S/Au interface,^{26,28} as shown by the appearance of MSH_2^+ ($m/z = 61, 97, 141$, respectively)

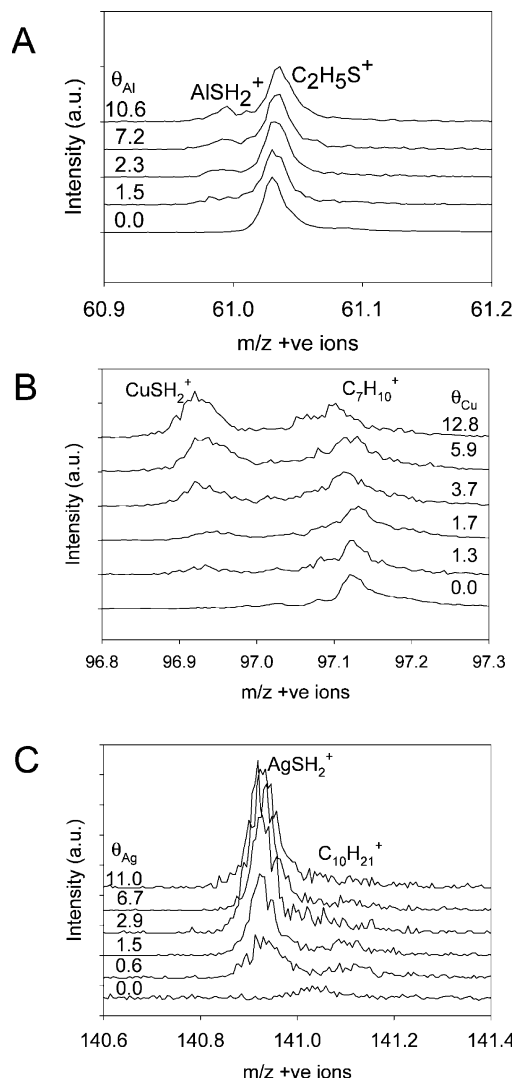


Figure 2. High-resolution SIMS spectral overlays of MSH_2^+ fragments. A, B, and C represent positive ions of nominal mass 61, 97, and 141 amu. The intensities in plots A, B, and C are normalized to the initial peak intensity of $\text{C}_2\text{H}_5\text{S}^+$, $\text{C}_7\text{H}_{13}^+$, and $\text{C}_{10}\text{H}_{21}^+$, respectively.

peaks (Figure 2) and $\text{Au}_x\text{M}_y\text{S}_z^-$ cluster ions (data not shown) for increasing increments of Al, Cu, and Ag deposition. In Figure 2, the intensities of the MSH_2^+ ($m/z = 61, 97, 141$, respectively) peaks are shown for increasing increments of Al, Cu, and Ag deposition. The AlSH_2^+ , CuSH_2^+ , and AgSH_2^+ spectra are normalized, respectively, to the initial peak intensities of $\text{C}_2\text{H}_5\text{S}^+$, $\text{C}_7\text{H}_{13}^+$, and $\text{C}_{10}\text{H}_{21}^+$ to make obvious the changing intensities of the peaks with respect to the hydrocarbon and substrate fragments as the deposition progresses. The increase of the relative MSH_2^+ and $\text{Au}_x\text{M}_y\text{S}_z^-$ intensities throughout the low coverage deposition regime indicates the deposited metal atoms continuously penetrate all coverages to the Au/S interface. Note the important contrast to the case of Al metal deposition on a CH_3 -terminated SAM where penetration is observed to cease after an $\sim 1:1$ Al/Au adlayer forms.²⁶

The state of the penetrated metal atoms is revealed by the observation that the monomer (M^+), dimer (M_2^+), and trimer (M_3^+) peak intensities (where $M = \text{Al, Cu, Ag}$), shown in Figure 3, increase proportionately with the first increment of deposited metal increase. Earlier we demonstrated that these signals differ between systems where deposited Al chemisorbs at the mono-

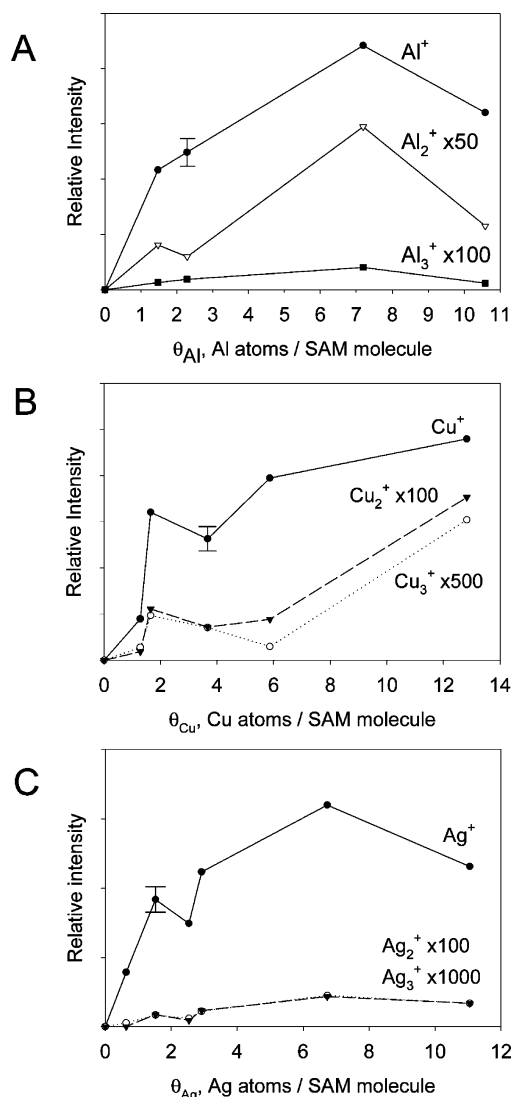


Figure 3. Integrated SIMS ion peak areas plotted versus θ_M for the OCH_3 SAM. A, B, and C represent the peak areas of Al_n^+ , Cu_n^+ , and Ag_n^+ , where $n = 1-3$, respectively. The single error bar shown is representative of the uncertainty for each datum.

layer terminus and those where it penetrates through the monolayer to the S/Au interface.^{26–28} When Al is first deposited onto a $-\text{CH}_3$ terminated SAM, which allows penetration, the Al^+ and Al_2^+ ions increase steadily, whereas there is a slight delay in the Al_3^+ ion. In contrast, for the $-\text{CO}_2\text{CH}_3$ terminated SAM, when the first increments of Al are deposited on the monolayer (where Al chemisorbs) there is an increase in the Al^+ intensity, while there is a slight delay in the growth of the Al_2^+ and Al_3^+ ion intensities, which rise in tandem. Following this interpretation, the early growth of M_2^+ intensities support the conclusion that Al, Cu, and Ag penetrate through the $-\text{OCH}_3$ terminated SAM to the Au/S interface.

After deposition of Al, Cu, or Ag, another important diagnostic feature in the TOF SIMS spectra is the relatively consistent intensity of the Au_2A^- and AuA_2^- peaks, which involve intact adsorbate molecules. Note in Figure 4 how the areas of these peaks barely drop below their initial values at continued Al, Cu, or Ag deposition (10.6, 27.0, and 16.2 ML, respectively), indicating that the deposition of the metal leaves the adsorbate molecule chemically intact and thus does not react

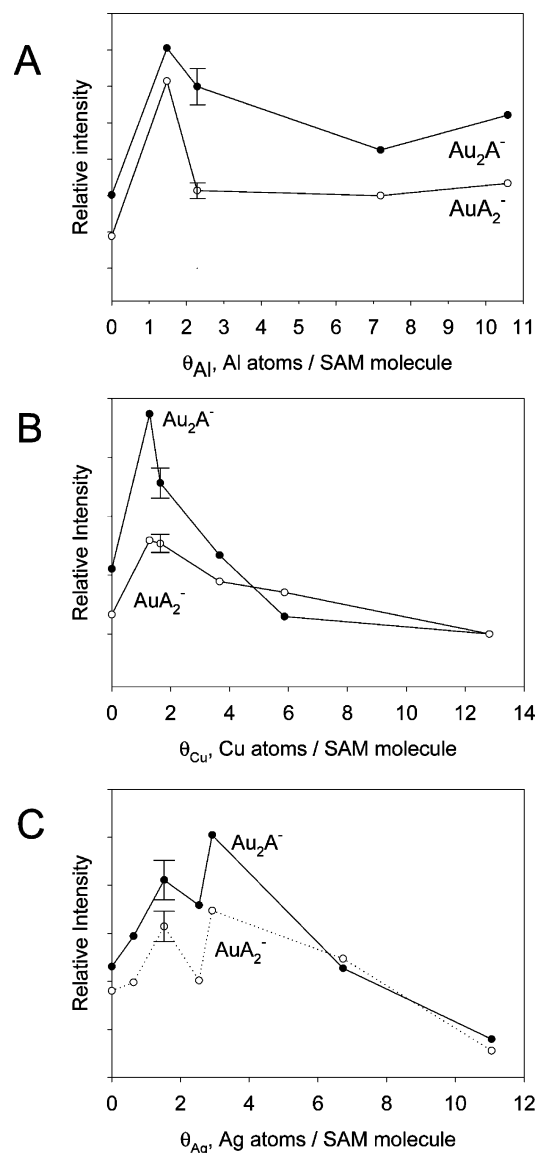


Figure 4. Integrated SIMS peak areas of Au_2A^- and AuA_2^- plotted versus θ_{Al} (A), θ_{Cu} (B), and θ_{Ag} (C). The single error bar shown is representative of the uncertainty for each datum.

with the $-\text{OCH}_3$ groups. In fact, the molecular ion peak intensities actually increase upon metal deposition, which is likely due to electron transfer, with increased ion yield, from the more electropositive deposited metal atoms to the more electronegative Au atoms and clusters leaving the surface.²⁶ Consistent with the lack of decrease of the molecular ion peak intensity, the hydrocarbon fragment peak intensities remain relatively unchanged during the early stages of the deposition (data not shown), as do the metal cluster peaks involving the Au substrate. As the deposition progresses, all peak intensities become increasingly attenuated, consistent with a growing metal overlayer that can block substrate ion ejection.

3.1.2. Deposition of Au. In the positive ion mass spectrum, the absence of AuOCH_3^+ and AuO^\pm ions (data not shown) indicates that the Au atoms do not interact with the terminal $-\text{OCH}_3$ group. We do conclude, however, from the appearance of the AuSH_2^+ peak intensity, shown in Figure 5a, that deposited Au atoms penetrate to the Au/S interface. Penetration through the SAM is supported by STM measurements of Ohgi et al.,⁶¹

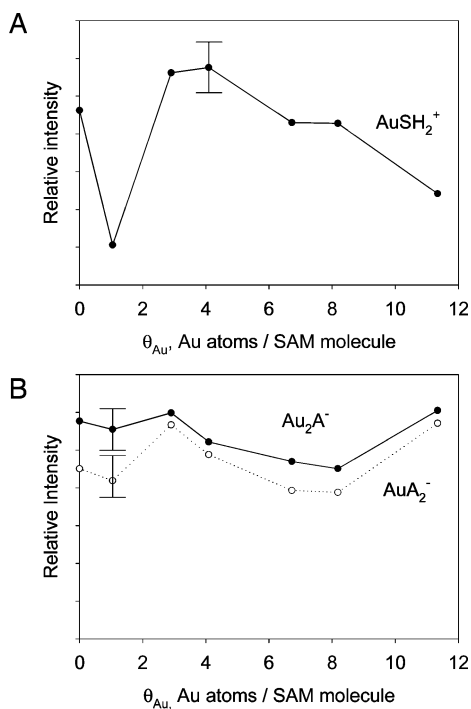


Figure 5. Integrated SIMS peak intensities of (a) $AuSH_2^+$ and (b) Au_2A^- and AuA_2^- . The single error bar shown is representative of the uncertainty for each datum.

who reported that deposition of Au atoms on an octanethiolate ($CH_3(CH_2)_7S-$) on Au{111} forms islands at the Au/S interface. At $\theta_{Au} \approx 6-7$, these islands were observed to coalesce into a smooth surface. Such morphology changes lead to changes in the observed secondary ion mass spectra. The initial surface roughening will lead to the formation of Au moieties with a lower coordination, which should make the ejection and ionization of departing fragments and clusters easier. Once the surface is smoothed upon continued Au deposition, the efficiency of the ejection/ionization of Au clusters and fragments is reduced. Indeed, the data, shown in Figure 5a, do follow this trend of increasing and then decreasing $AuSH_2^+$ peak intensities.

Since a new Au adlayer is being formed, one would expect the deposited Au atoms to continuously penetrate through the SAM layer to the Au/S interface. The relatively constant intensities of the AuA_2^- and Au_2A^- ions, which involve intact adsorbate molecules, support this behavior (Figure 5b; the variation in the intensity is mainly due to integration errors ($\sim 10\%$ absolute ratio)). Even after a deposition of $\theta_{Au} \approx 124$, the Au_2A^- and AuA_2^- yields are $\sim 70\%$ of those of the bare monolayer, indicating that there is little or no Au overlayer formation even at this high coverage. Therefore, these data confirm that Au is penetrating through the monolayer throughout the deposition range with no metallic overlayer forming. Hence, the $-OCH_3$ terminated SAM “floats” on top of the deposited Au interlayer.

3.2. IRS. The IR assignments for the bare monolayer have been reported previously.^{28,42} Relevant peaks in the low- and high-frequency ranges, 750–1600 cm^{-1} and 2700–3100 cm^{-1} , respectively, are summarized here for reference. The peaks at 1132, 1390, and 1465 cm^{-1} are assigned as the C–O–C antisymmetric stretch (ν_{C-O}), the $-CH_3$ symmetric deformation

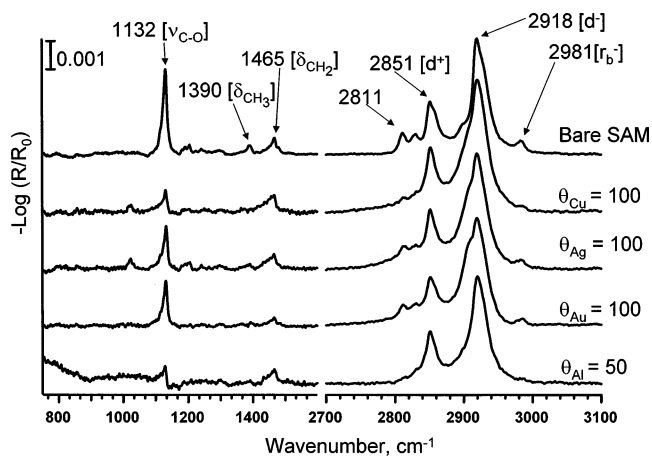


Figure 6. Low- and high-frequency region IRS spectra of the bare OCH_3 SAM and upon Al, Cu, Ag, and Au deposition.

(δ_{CH_3}), and the $-CH_2-$ scissor deformation (δ_{CH_2}), respectively. In the high-frequency regime, the $-CH_2-$ d^+ and d^- stretches are assigned at 2851 and 2918 cm^{-1} , and the peaks at 2811, 2828, and 2981 cm^{-1} are the various stretching modes of the terminal CH_3 group. The data indicate that the bare monolayer is well-organized, with the chains primarily in an all trans conformation.³⁹

The IR spectra of the monolayer before and after metallization with Cu, Ag, and Au at $\theta_M = 100$ ($M = Cu, Ag, Au$) and Al at $\theta_{Al} = 50$ are shown in Figure 6. In each case, we observe the preferential attenuation of the modes associated with the $-OCH_3$ group. The observed attenuation is more pronounced upon deposition of Al than upon Cu, Ag, and Au deposition. At $\theta_{Al} = 50$, the intensity of ν_{C-O} (1132 cm^{-1}) has been reduced by $\sim 80\%$ of its original value, the intensity of δ_{CH_3} (1390 cm^{-1}) has disappeared into the baseline noise, and there is a significant loss of intensity of modes associated with the CH_3 group (2811, 2828, and 2981 cm^{-1}). In contrast, the intensities of the $-CH_2-$ bend and stretch modes at 1465, 2851, and 2918 cm^{-1} show slight attenuation, but the retention of the peak positions indicates the monolayer chains are still well-ordered. Upon deposition of 100 mL of Cu, Ag, and Au, the intensity of ν_{C-O} mode is reduced by $\sim 75\%$, $\sim 50\%$, and $\sim 50\%$, respectively, of its original value. It is also observed that the intensity of δ_{CH_3} has disappeared into the baseline noise and that there is a slight attenuation of the CH_3 modes. The intensities of the $-CH_2-$ bend and stretch modes are also slightly attenuated but, as with deposition of Al, indicate the chains remain well-ordered. We also note that upon deposition of Cu, Ag, and Au, a shoulder on the low-frequency side of the $-CH_2-$ d^- mode (~ 2906 cm^{-1}) grows in, while upon deposition of Cu and Ag a second small feature grows in at 1022 cm^{-1} . An experiment using $HS-(CH_2)_{16}-OCD_3$ monolayers indicates that the feature at 2906 cm^{-1} is due to the methylene backbone of the SAM and not the terminal methoxy group. To date, however, we have not been able to rigorously assign these modes.

The attenuation of IR modes can be caused by chemical reactions, reorientation of the monolayer dipoles with respect to the surface,³⁹ or by screening of the dipoles due to metal atoms, clusters, or overlayers.² Since we do not observe the appearance of new absorption bands, such as the Al–O stretch (855 cm^{-1}),^{26–28} and given the TOF SIMS results, we can

(61) Ohgi, T.; Sheng, H.-Y.; Dong, Z.-C.; Nejjoh, H. *Surf. Sci.* **1999**, *442*, 277–282.

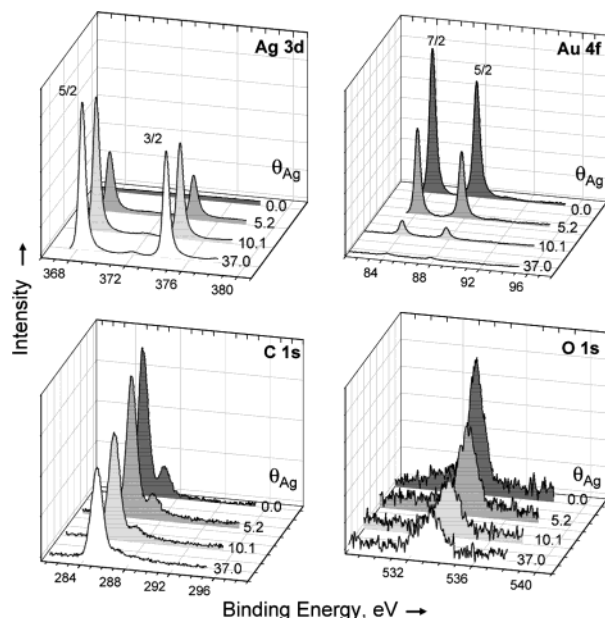


Figure 7. XPS spectra (15° takeoff angle from the sample surface) of the C1s, O1s, Au4f, and Ag3d core levels for an $-\text{OCH}_3$ SAM prior to and following deposition of Ag.

eliminate chemical reactions as a cause. Further information is needed to separate the other two mechanisms.

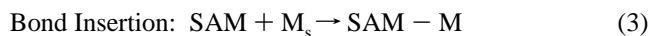
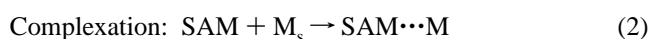
3.3. XPS. As a qualitative complement to the TOF SIMS and IRS characterizations, a few XPS experiments were made for the case of Ag deposition on the $-\text{OCH}_3$ terminated SAM in which competing Au/S substrate penetration and overlayer deposition were observed. Since both Cu and Ag behave similarly, the XPS experiments for the case of Ag deposition serve as a check for the characteristics of both cases. The data were taken at a photoelectron takeoff angle of 15° from the sample surface to emphasize the signals from the outer (vacuum) sample surface. The results, summarized in Figure 7, show three main features. First, as expected, the continued deposition of Ag results in increasing intensities of the Ag 3d core level peaks as the metal deposition continues. Second, the C 1s, O 1s, and Au 4f peaks decrease in intensity with increasing Ag coverage, consistent with the Ag increasingly covering the sample surface. Third, the C 1s and O 1s peaks attenuate much less with increasing Ag coverage than the Au 4f peak. In the limit of exclusive penetration of the deposited Ag metal atoms, the C 1s and O 1s peaks would not attenuate while the Au 4f intensity would eventually vanish. Conversely, at the other limit of exclusive Ag overlayer formation all three core levels, Au 4f, C 1s, and O 1s, would attenuate in a similar way. Given the observed behavior of these attenuation rates between the limiting cases, the XPS data are consistent with the TOF SIMS and IRS conclusions that a fraction of the Ag is deposited at the SAM/vacuum surface, with the remainder penetrating to cover the Au substrate.

The C 1s core level spectra of the $-\text{CH}_2\text{OCH}_3$ carbons ($\sim +2.0$ eV shifted from the main $-\text{CH}_2-$ alkyl chain peak in Figure 7) reveal perturbations of the ether group by deposited Ag. Note the broadening and merging with the main $-\text{CH}_2-$ alkyl chain peak with increasing Ag coverage. Since these effects occur more rapidly than attenuation of the main $-\text{CH}_2-$ peak, this observation is consistent with a complexation or solvation of the methoxy group by Ag atoms, as indicated by

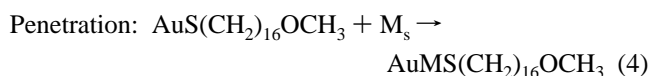
the TOF SIMS data. Although there is some slight shifting of the O 1s peak positions and shapes with Ag coverage, the effects are comparatively small compared to the C 1s changes.

4. Discussion

4.1. Overall Reaction Pathways. All the present data for Cu, Ag, and Au and the previous data for Al^{26–28,36} are consistent with a general mechanism in which the deposited metal atoms can (a) interact with the terminal group and stabilize at the SAM surface,^{28,36} (b) penetrate through the film,^{21,26,28} or both. In addition, the metals may (c) react with the terminal group while preserving the SAM methylene backbone,^{19,26,27} (d) react with and destroy the monolayer, an obviously undesirable result,^{19,62} or (e) exhibit a combination of these mechanisms.^{28,36} These reaction pathways can be summarized as follows:



(Organometallic formation)



where M_g and M_s represent the deposited metal atoms in the vapor and surface adsorbed states, respectively, and SAM denotes the alkanethiolate adsorbed on the Au surface, $\text{AuS}(\text{CH}_2)_{16}\text{OCH}_3$. While the adsorption mechanism 1 is considered to be reversible, our results, in particular TOF SIMS data, indicate that the metal atoms do not desorb from the SAM surface during the experiment.⁶³ The equilibrium in step 2 implies that the adsorbed metal atoms can rapidly diffuse between preferred sites at the SAM/vacuum interface.

The experimental data indicate that the deposited Al, Cu, and Ag atoms do not insert into the $-\text{OCH}_3$ group to form a $M-\text{O}$ bond but interact with the methoxy terminal group and therefore reaction pathway 2 is operative (see section 4.2 below). The data also indicate that the deposited Al, Cu, and Ag metal atoms penetrate to the Au/S interface (pathway 4). For Au metal deposition, the metal atoms only penetrate to the Au/S interface, and hence, mechanisms 1 and 4 are operative.

A schematic diagram of the overall deposition processes, deduced from the experimental data, is shown in Figure 8.

4.2. Specific Interactions (Solvation) of Deposited Metal Atoms with the $-\text{OCH}_3$ Group. Following condensation of the metal atoms on the SAM surface (step 1) the evolution of the metal–SAM interaction is governed by the interplay of the localization of the metal atoms at the $-\text{OCH}_3$ groups (step 2), overlayer film nucleation and growth, and penetration to the Au/S interface (step 4). The presence of MOCH_3^+ ions, where $M = \text{Al, Cu, Ag}$, and not $\text{M}_x\text{O}_y^{\pm}$ ions in the TOF SIMS spectra (Figure 1), demonstrates a $M \cdots \text{OCH}_3$ association, consistent

(62) Konstadinis, K.; Zhang, P.; Opila, R. L.; Allara, D. L. *Surf. Sci.* **1995**, *338*, 300–312.

(63) In contrast, we have observed that other deposited metal atoms, e.g., Mg, do desorb with a high probability from the $-\text{OCH}_3$ SAM surface under similar deposition conditions to the present experiments. Walker, A. V.; Tighe, T. B.; Cabarcos, O.; Haynie, B. C.; Allara, D. L.; Winograd, N. To be submitted for publication.

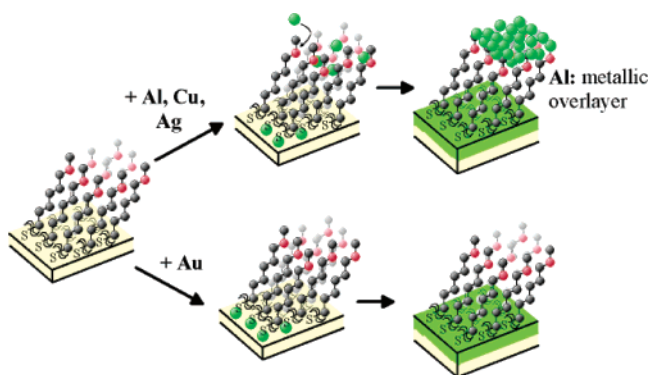


Figure 8. Schematic illustrations of the important features of the reaction pathways, including the steric hindrance of the metal–oxygen interaction. Metal atom is represented in green, oxygen in red, and hydrocarbons in black.

with the presence of a stabilizing interaction between the Al, Cu, and Ag atoms and the $-\text{OCH}_3$ group but not insertion into the $\text{O}-\text{CH}_3$ bond. Further evidence that the deposited metal atoms do not insert into the terminal group is the nearly constant character (i.e., the peak shape and position) of the $\text{C}-\text{O}$ stretch mode at 1132 cm^{-1} (Figure 6). We note that this interaction is sufficiently strong to localize metal atoms on the surface such that subsequent nucleation and growth of a metal overlayer may occur, but sufficiently weak so that penetration of the metal atoms remains competitive. Thus, the reaction is analogous to a weak solvation.

In the case of Cu and Ag, the localization and penetration of metal atoms appear to be balanced such that both processes occur continuously (see section 4.2 below). In the case of Al atoms, both localization at the vacuum interface and penetration occur initially, but at higher metal coverages the penetration ceases and a metallic overlayer forms.^{28,36} The detailed electronic and steric nature of the $\text{M}\cdots\text{OCH}_3$ interaction is quite subtle as evidenced by the $\text{Ag}\cdots\text{OCH}_3$ interaction. On one hand, upon Ag deposition, the $\text{C}-\text{O}$ stretching vibration, a general measure of the bond strength, is barely perturbed at low coverages (Figure 6). In contrast, the $-\text{CH}_2\text{OCH}_3$ C1s XPS spectra (Figure 7), a measure of the local electron density around the ether carbons, show obvious perturbations by deposited Ag atoms.³⁶ These subtle metal-methoxy interactions are similar to the case of Al deposition,²⁸ where it was concluded that solvation or complexation types of perturbations arise.

Quantum mechanical calculations were made on the isolated model systems $\text{M} + \text{CH}_3\text{OCH}_3$ and $\text{CH}_3\text{CH}_2\text{CH}_3$, where $\text{M} = \text{Al}, \text{Cu}, \text{Ag},$ and Au , to investigate the energetics of the stabilization process (Table 1). Previous calculations on the $\text{Al}-\text{OCH}_3$ interaction at the B3PW91/6-311+G(2df,p) level of theory²⁸ demonstrated that the lowest energy configuration, -272 kJ mol^{-1} , involves the *insertion* of Al into the $\text{C}-\text{O}$ bond, with a lesser minimum of -89 kJ mol^{-1} for $\text{C}-\text{C}$ bond insertion. Since neither of these processes is observed experimentally, it was assumed that the activation barriers for these processes are prohibitively high.²⁸ In the present study, calculations for insertion of Cu, Ag, and Au into the $\text{C}-\text{O}$ and $\text{C}-\text{C}$ bonds demonstrate that these complexes are unstable and thus would not be observed, in agreement with experimental data.

For these systems, however, secondary minima at -52 , -34 , -13 , and -17 kJ mol^{-1} are found for complexation between Al, Cu, Ag, and Au and the O atom of the $-\text{OCH}_3$, respectively (Table 1). Note that while Au shows greater stabilization by

Table 1. DFT Calculated Stabilization Energies for Various Metal–Oxygen Complexes

Molecule	Complex	Metal	Stabilization Energy (kJ/mol)	
			LANL2DZ	6-311-G(2df,p)
	$\text{O}\cdots\text{Al}$	Al	-52	-33
$\text{CH}_3-\text{O}-\text{Al}-\text{CH}_3$	$\text{O}-\text{Al}-\text{C}$	Al	-261	-272
$\text{C}_2\text{H}_5-\text{Al}-\text{CH}_3$	$\text{C}-\text{Al}-\text{C}$	Al	-69	-90
	$\text{O}\cdots\text{Cu}$	Cu	-34	
$\text{CH}_3-\text{O}-\text{Cu}-\text{CH}_3$	$\text{O}-\text{Cu}-\text{C}$	Cu	Failed	
$\text{C}_2\text{H}_5-\text{Cu}-\text{CH}_3$	$\text{C}-\text{Cu}-\text{C}$	Cu	48	
	$\text{O}\cdots\text{Ag}$	Ag	-13	
$\text{CH}_3-\text{O}-\text{Ag}-\text{CH}_3$	$\text{O}-\text{Ag}-\text{C}$	Ag	Failed	
$\text{C}_2\text{H}_5-\text{Ag}-\text{CH}_3$	$\text{C}-\text{Ag}-\text{C}$	Ag	142	
	$\text{O}\cdots\text{Au}$	Au	-17	
$\text{CH}_3-\text{O}-\text{Au}-\text{CH}_3$	$\text{O}-\text{Au}-\text{C}$	Au	Failed	
$\text{C}_2\text{H}_5-\text{Au}-\text{CH}_3$	$\text{C}-\text{Au}-\text{C}$	Au	52	

the $-\text{OCH}_3$ group than Ag, Au exclusively penetrates to the Au/S interface. This situation implies an activation barrier for $\text{Au}-\text{OCH}_3$ stabilization relative to the Ag case. Al, Cu, and Ag all prefer to bind near the O atom, away from the $\text{C}-\text{O}-\text{C}$ bonds. Geometric considerations indicate that this optimum isolated cluster geometry will be unfavorable in the SAM due to steric hindrances at the SAM/vacuum interface (Figure 8). While a small number of $-\text{OCH}_3$ groups may be able to reorient to accommodate optimal $\text{M}\cdots\text{OCH}_3$ interactions, most terminal groups will not be able to reorient due to molecular packing in the SAM. Thus, we expect that the average stabilization energy per deposited metal atom will be considerably reduced relative to the isolated system. This picture is consistent with the minor perturbations observed in the IR $\text{C}-\text{O}$ stretching frequencies (Figure 6). Given the low rotational barrier of the $\text{RC}(\text{H}_2)-\text{OCH}_3$ bond relative to the $\text{C}-\text{C}$ bonds,²⁸ a wide range of $\text{M}\cdots\text{OCH}_3$ geometries are possible (Figure 7). Thus, the metal surface interaction can be considered as a quasi-isotropic weak solvation of the metal by the $-\text{OCH}_3$ terminal group, as suggested previously for the case of Al.⁶⁴

4.3. Penetration to the Au/S Interface. The experimental data indicate that the deposited metal atoms penetrate to the Au/S interface since in the TOF SIMS spectra, we observe peaks of the form MSH_2^+ where $\text{M} = \text{Al}, \text{Cu}, \text{Ag},$ or Au . In this discussion, it is useful to refer to the schematic in Figure 9, which summarizes important aspects of the metal penetration process.

In refs 22 and 28, it was concluded, primarily from the TOF SIMS data, that for the $-\text{CH}_3$ terminated SAM, penetration of Al atoms ceases to increase at $\theta_{\text{Al}} \approx 2.7$, at the onset of Al overlayer growth at the SAM/vacuum interface. In contrast, for the $-\text{OCH}_3$ SAM case, penetration continues even at $\theta_{\text{Al}} \approx 12.2$. This behavior was explained on the basis that the penetration of Al atoms to the Au/S interface continues until an $\sim 1:1$ Al/Au adlayer is formed, after which the penetration path closes and further deposited metal atoms form an overlayer

(64) We have evidence that the orientation of the $-\text{OCH}_3$ group does change the apparent reactivity of deposited metal atoms. An indication of the orientation of the methoxy group relative to the methylene backbone is given by the ratio of the intensity of the $\text{d}^- \text{CH}_2$ stretch (2918 cm^{-1}) to the $\text{C}-\text{O}$ stretch (1132 cm^{-1}). Upon Al deposition for a SAM layer with a ratio of 1:2 ($\text{d}^- \text{CH}_2$ str.: $\text{C}-\text{O}$ str.), larger changes in the IR spectra are observed than for a layer with a 1:1 ratio, indicating that the deposited Al has apparently different reactivities depending upon the orientation of the methoxy group.

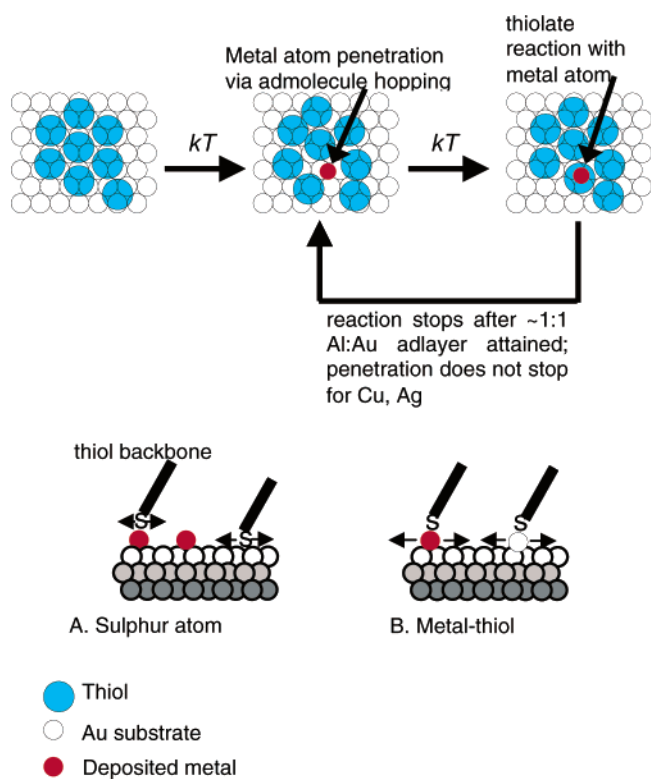


Figure 9. Cartoon illustrations of thiol (sulfur atom) or M–Th, where M = metal atom and Th = thiol, diffusion across the Au surface.

at the SAM/vacuum interface. It is reasonable to assume that the penetration path also closes for the $-\text{OCH}_3$ case if sufficient Al were deposited to produce an $\sim 1:1$ Al/Au interfacial layer because the $-\text{CH}_3$ and $-\text{OCH}_3$ groups should have a negligible effect on the characteristics of the S/Au interface, located 16 C atoms from the chain terminus. Indeed, at a coverage of $\theta_{\text{Al}} \approx 192$, the TOF–SIMS data indicate that a metallic Al overlayer has formed and that the $-\text{OCH}_3$ SAM has been completely covered by the deposited Al. Further, previous XPS data²⁸ also indicate that Al ceases to penetrate to the Au/S interface at lower coverages, while further increments of deposited Al atoms form a metallic overlayer. The penetration mechanism was proposed to occur via the thermally driven translational motion (hopping) of the adsorbate molecules on the Au substrate lattice, which leads to the transient appearance of holes (defects) sufficiently large to provide channels for metal atom diffusion to the S/Au interface (see the upper part of Figure 9).

In contrast, at very high metal coverages, Cu, Ag, and Au atoms continue to penetrate to the S/substrate interface with formation of a thickening layer of the deposited metal on top of the original Au substrate surface. This can be seen from the TOF SIMS data, which show significant peak intensities of both cluster and fragment ions associated with the SAM at $\theta_{\text{Cu}} \approx 176$, $\theta_{\text{Ag}} \approx 130$, and $\theta_{\text{Au}} \approx 124$. For example, at $\theta_{\text{Cu}} \approx 176$ the intensities of CuSH_2^+ (penetration) and CuOCH_3^+ ($\text{Cu}-\text{OCH}_3$ interaction) are $\sim 80\%$ of the observed maximum peak intensity, and at $\theta_{\text{Ag}} \approx 130$ the intensities of AgSH_2^+ and AgOCH_3^+ are $\sim 85\text{--}90\%$ of the observed maximum peak intensity. The XPS data further show for the case of Ag (Figure 7) that the Au 4f substrate signals attenuate much faster with increasing Ag deposition than the C 1s and O 1s SAM signals. Thus, the SAM is covered by only a fraction of the deposited Ag compared to the Au substrate which is buried beneath all the Ag.

4.3.1. Mechanism. A satisfactory model for the penetration pathway must be able to explain (a) why the Al penetration channel is closed after $\sim 1:1$ Al/Au adlayer has formed but (b) why the penetration of Cu, Ag, and Au continues even at very high metal coverages. Our previously proposed penetration mechanism involved the diffusion of metal adatoms from the vacuum surface to lower energy positions at the Au/S interface.^{22,28,65} In the case of Al, as the Al atoms accumulate at the Au/S interface, and they were proposed to insert into the Au–SR bonds (R = alkyl) to form Al–SR bonds. If the formation of these bonds slows or stops the formation of transient defects, this would explain the closure of the penetration channel upon completion of $\sim 1:1$ Al/Au adlayer. A schematic figure of this process is shown in Figure 9.

If this mechanism is correct, the different observed behaviors for Al, Cu, Ag, and Au must correlate with the energetics of the diffusing species. Specifically, the central issue is whether the lowest energy pathway for the lateral motion of the SAM moiety is motion of a metal–alkanethiolate ($-\text{MSR}$) across the Au substrate surface (or metal adlayer at high coverages) or motion of an alkanethiolate moiety ($-\text{SR}$) across the metal adlayer (M) surface. To examine these possibilities, one must estimate the activation barriers for lateral hopping (diffusion) of these species. An easy way to do this is to assume that these activation barriers correlate with the different bond energies involved, either M–SR or Au–MSR (M–MSR at higher coverages).

Using ultraviolet photoelectron spectroscopy, XPS, and work function measurements, Shen and Nyberg suggested that the Al–SR bond is weaker than the Cu–SR bond.⁶⁶ Since the penetration of Cu continues well past the formation of an $\sim 1:1$ M/Au adlayer in contrast to the case of Al where penetration ceases, it is apparent that formation of Cu–SR bonds is much less efficient at closing the penetration channel. This would rule out the alkanethiolate ($-\text{SR}$) chain hopping model in favor of the metal–alkanethiolate diffusion model.

To investigate in more detail the energetics of the alkanethiolate ($-\text{S}$ atom) hopping model, quantum mechanical calculations were applied to the isolated model system $\text{M}-\text{S}(\text{CH}_2)_5-\text{OCH}_3$ where M = Al, Cu, Ag, Au. The results are summarized in Table 2. If $E_{\text{M}-\text{S}} > E_{\text{Au}-\text{S}}$, where E = bond dissociation energy, the metal atom should insert into the Au–S bond to form a Au–M–SR structure, and the penetration of the deposited metal atoms will cease after $\sim 1:1$ metal–Au adlayer has been attained. For Ag, $E_{\text{Ag}-\text{SR}} = 173 \text{ kJ mol}^{-1}$ is close to $E_{\text{Au}-\text{SR}} = 179 \text{ kJ mol}^{-1}$, and thus (in agreement with experiment), one would expect that the penetration pathway would not close since the barrier for the lateral diffusion of $-\text{SR}$ species will remain approximately the same before and after deposition. However, for Al and Cu, $E_{\text{Al}-\text{SR}}$ and $E_{\text{Cu}-\text{SR}} = 292$ and 227 kJ mol^{-1} , respectively, are both larger than $E_{\text{Au}-\text{SR}} = 179 \text{ kJ mol}^{-1}$. Hence, in agreement with the observed experimental data, both Cu and Al will insert into the Au–SR bond. However, if $-\text{SR}$ diffusion across the surface were occurring then one would also predict that penetration of deposited Cu atoms would cease after an $\sim 1:1$ adlayer has been attained, in

(65) The formation of transient defects and the subsequent diffusion of species is a common mechanism; such processes are operative for the diffusion of gases and other species through polymers (*Diffusion in Polymers*; Crank, J., Park, G. S., Eds.; Academic Press: New York, 1968) and along interfaces (Sutton, A. P.; Balluffi, R. W. *Interfaces in Crystalline Materials*; Clarendon Press: Oxford, 1995).

(66) Shen, W.; Nyberg, G. L. *Surf. Sci.* **1993**, *296*, 49–56.

Table 2. DFT Calculated Bond Energies for Various Metal–Thiol Complexes^a

complex	metal	binding energy (kJ/mol)	S–M distance (Å)	M1–M2 distance (Å)
CH ₃ O(CH ₂) ₅ S–Au	Au	179	2.36	
CH ₃ O(CH ₂) ₅ S–Al	Al	293	2.36	
CH ₃ O(CH ₂) ₅ S–Ag	Ag	174	2.42	
CH ₃ O(CH ₂) ₅ S–Cu	Cu	228	2.20	
CH ₃ O(CH ₂) ₅ S _{Au} –Au	Au	118	2.40	Au–Au = 2.56
CH ₃ O(CH ₂) ₅ S _{Au} –Al	Al	200	2.45	Au–Al = 2.46
CH ₃ O(CH ₂) ₅ S _{Al} –Au	Au	164	2.29	Al–Au = 2.43
CH ₃ O(CH ₂) ₅ S _{Al} –Al	Al	78	2.31	Al–Al = 2.78
CH ₃ O(CH ₂) ₅ S _{Au} –Ag	Ag	97	2.42	Au–Ag = 2.64
CH ₃ O(CH ₂) ₅ S _{Ag} –Au	Au	95	2.48	Ag–Au = 2.62
CH ₃ O(CH ₂) ₅ S _{Ag} –Ag	Ag	83	2.63, 2.65	
CH ₃ O(CH ₂) ₅ S _{Au} –Cu	Cu	128		
CH ₃ O(CH ₂) ₅ S _{Cu} –Au	Au	124	2.23	Cu–Au = 2.42
CH ₃ O(CH ₂) ₅ S _{Cu} –Cu	Cu	123	2.38, 2.39	

^a Most of the metal dimer complexes form a chain structure: S–M1–M2. These two structures, however, have both metals complexed directly to the sulfur atom.

conflict with the observed continuous penetration of Cu atoms. This supports metal–alkanethiolate (–MRS) diffusion as the critical step for closure of the penetration pathway (Figure 7). Support for this mode of surface diffusion is given by results of previous STM studies in which gold–alkanethiolate moieties (Au–SR) have been observed to diffuse across an Au{111} surface.^{67,68}

Calculations for the isolated model system M + AuS(CH₂)₅–OCH₃ (AuSR), where M = Al, Cu, Ag, and Au, are summarized in Table 2 and support the metal–alkanethiolate diffusion mechanism. First we note that $E_{\text{Au–SR}}$ (179 kJ mol^{–1}) > $E_{\text{Au–AuSR}}$ (118 kJ mol^{–1}), which suggests that there is a lower energy barrier for diffusion of –AuSR than for –SR across the Au surface, in agreement with the STM data.^{67,68} For Al, Cu, and Ag, $E_{\text{M–SR}} = 293, 228, \text{ and } 174 \text{ kJ mol}^{-1}$, respectively, is larger than the gold metal–alkanethiolate bond energy, $E_{\text{Au–MSR}} = 164, 124, \text{ and } 95 \text{ kJ mol}^{-1}$, respectively, suggesting that the –MSR species controls surface diffusion across the Au substrate.

The remaining question of whether the penetration channel closes can be readily explained on the basis of the Au–MSR energies. First, since $E_{\text{Au–AlSR}}$ (164 kJ mol^{–1}) > $E_{\text{Au–AuSR}}$ (118 kJ mol^{–1}), one would expect that the rate of the diffusion of the alkanethiolate chains would rapidly decrease once the –AlSR species has formed at the Au/S interface, and thus penetration of deposited Al atoms will cease after an ~1:1 Al/Au adlayer has been attained. Second, since $E_{\text{Al–AlSR}}$ (78 kJ mol^{–1}) < $E_{\text{Au–AlSR}}$ (164 kJ mol^{–1}), it is energetically unfavorable for a second adlayer of aluminum to be deposited. Finally, we also note that $E_{\text{Al–AuSR}}$ (200 kJ mol^{–1}) > $E_{\text{Au–AlSR}}$ (164 kJ mol^{–1}). However, it is unlikely that there would be an exchange in the Au and Al atoms at the interface since this interaction is endothermic,⁶⁹ viz., $\text{Au–Al–S(CH}_2)_5\text{OCH}_3 \rightarrow \text{Al–Au–S(CH}_2)_5\text{OCH}_3$ $\Delta E = 78 \text{ kJ mol}^{-1}$.

For Cu and Ag, $E_{\text{Au–MSR}}$ is 124 and 95 kJ mol^{–1}, respectively, and is similar to that for Au $E_{\text{Au–AuSR}} = 118 \text{ kJ mol}^{-1}$. Hence, one would not expect the rate of the diffusion of the alkanethiolate chains to vary much between the Au, Au–Cu, and Au–

Ag interfaces, and thus the metal penetration pathway would not close, as observed in our experiments. We also note that $E_{\text{M–MSR}}$, where M = Cu, Ag, is approximately $E_{\text{Au–MSR}}$; thus, there is no energy barrier to the continued deposition of metal atoms at the sulfur/substrate interface.

5. Conclusions

Upon vapor deposition of aluminum, copper, and silver onto a –OCH₃ terminated hexadecanethiolate SAM on Au{111}, the metal atoms simultaneously penetrate to the Au/S interface, where a stable adlayer forms, and stabilization at –OCH₃ groups occurs, leading to overlayer nucleation at the vacuum interface. In the case of Al, the penetration channel closes after ~1:1 Al/Au adlayer has been attained, similar in overall character to the previously studied case of a –CH₃ terminated SAM.²⁶ In contrast, for Cu and Ag deposition the penetration channel does not close. To explain these observations, we propose that the penetration occurs via transient defects that arise from thermally activated diffusion of metal–alkanethiolate moieties, –MSR where M = Au, Al, Cu and Ag and R = (CH₂)₁₆OCH₃. As the deposition progresses, deposited metal atoms accumulate at the Au/S interface and insert into the Au–SR bonds to form M–SR bonds. Upon deposition of Al, the Au–AlSR bond is stronger than the Au–AuSR bond and thus has a higher energy barrier to diffusion, eliminating or greatly reducing the formation of transient defects. Upon completion of ~1:1 Al/Au adlayer, the penetration channel closes, and further deposited Al atoms form an overlayer at the SAM/vacuum interface. In contrast, the Au–AgSR and Au–CuSR bond strengths are weaker or about the same strength as the Au–AuSR bond. Thus, these moieties are able to diffuse across the surface, leading to the formation of transient defects, and hence, penetration to the S/substrate interface continues at all metal coverages.

Finally, gold, an almost inert metal, does not interact with the methoxy terminal group. Rather, penetration of deposited Au atoms to the Au/S interface is observed at all coverages studied, which leads to the interesting result of a “floating” SAM.

Experiments are underway to further examine the crucial details of these metal deposition mechanisms, including in situ atomic force microscopy to characterize the lateral distribution of the overlayer metal, cooling experiments to characterize the temperature-dependent behavior of the competition between penetration and overlayer formation, and varying the alkanethiolate chain length from even to odd numbers of CH₂ groups to alter the steric environment of the terminal –OCH₃ group.

This study, in conjunction with previous studies,^{26–28} provides a basis for the rational design and control of many types of metallized organic structures ranging from metallized polymer surfaces, with strong metal adhesion and controlled morphology, to highly optimized electrical contacts in organic and molecular electronic devices.

Acknowledgment. We acknowledge financial support from DARPA and the National Science Foundation. A.V.W. would also like to thank Lev Gelb for many useful discussions.

JA0395792

(69) The reaction energy is given by:

$$\begin{aligned} \Delta E &= E(\text{bonds made}) - E(\text{bonds broken}) \\ &= E(\text{Au} - \text{S(CH}_2)_5\text{OCH}_3) + E(\text{Al} - \text{AuS(CH}_2)_5\text{OCH}_3) - \\ &\quad E(\text{Al} - \text{S(CH}_2)_5\text{OCH}_3) - E(\text{Au} - \text{AlS(CH}_2)_5\text{OCH}_3) \\ &= -(179 + 200 - 293 - 164) \text{ kJ mol}^{-1} \end{aligned}$$

(67) Stranick, S. J.; Parikh, A. N.; Tao, Y.-T.; Allara, D. L.; Weiss, P. S. J. *Phys. Chem.* **1994**, *98*, 7636–7646.

(68) Terán Arce, F.; Vela, M. E.; Salvarezza, R. C.; Ariva, A. J. *Electrochim. Acta* **1998**, *44*, 1053–1067.